

# A new approach based on spectral graph theory to avoiding enclosed holes in topology optimization

A. Donoso, E. Aranda

*Departamento de Matemáticas,  
ETSII, Universidad de Castilla-La Mancha,  
Ciudad Real, Spain*

D. Ruiz

*Departamento de Matemáticas,  
EIIA, Universidad de Castilla-La Mancha,  
Toledo, Spain*

---

## Abstract

It is well-known that when maximizing the stiffness in structural design, several holes often appear distributed throughout the structure, leading to a distribution of the void phase that is not connected. Inspired by known results of spectral graph theory, this work proposes a new idea to prevent the appearance of those internal or encapsulated holes in topology optimized structures. The approach is density-based, where some sort of eigenvalue problem is solved in addition to the governing elasticity problem in each step of the iterative process. By means of the auxiliary eigenproblem, void phase connectivity may be imposed by constraining the second smallest eigenvalue, invariant known as algebraic connectivity in the context of graphs. Several examples in 2d and in 3d for minimum compliance are shown to corroborate our approach, thereby providing efficient performance together with improved manufacturability.

*Keywords:* graph theory, topology optimization, algebraic connectivity, enclosed holes

---

## 1. Introduction

Topology optimization (TO) [1] has become an imperative conceptual tool in structural design. It is of great help for designers in the not trivial task of

distributing a limited amount of material in a design space so as to optimize a certain objective function while some constraints are fulfilled. It is nevertheless true that sometimes implementing TO-based designs with conventional manufacturing processes becomes rather complicated. In this regard, additive manufacturing (AM) techniques have received special attention together with TO in the last decade ([2, 3]), as AM technologies make it possible to manufacture really complex structures directly from a computer. However, despite  
10 being cutting-edge 3d printing techniques, they are still some pending issues to be overcome. In this work, we focus on the structural connectivity issue, that is, to avoid the presence of enclosed holes in topology optimized structures, and in particular, in those of minimum compliance.

It is well-known that when minimizing the compliance (or maximizing the stiffness), different holes appear distributed throughout the structure in two-dimensional topologies, and it is also quite common in three-dimensional topologies, leading to a distribution of the void phase that is not connected. Although enclosed voids are desirable from a stiffness perspective, they are quite challenging or impossible to manufacture, specially when using AM ([2, 3]). This has  
20 motivated the development of constraint-based methods for topology optimization ([4, 5, 6, 7, 8]), among others, that help prevent the formation of enclosed holes in topology optimized structures.

As far as the authors' knowledge, there are not too many references to date regarding connectivity constrains in topology optimization problems, and all of them are relatively recent. The first strategy to tackle this issue was independently proposed for several authors in [9, 10, 11], and it was called the virtual temperature method (VTM). The idea consists in solving an auxiliary linear thermal problem where void is treated as conductive material, solid as  
30 insulator material and some parts of the boundary as heat sinks. There, void connectivity is imposed by constraining the maximum temperature in the void phase. Similar approaches have been used in fluid topology optimization to prevent enclosed (fluid-filled) pores that lead to singularities in the fluid analysis problem [12, 13]. Other extensions of this method are [14] to consider molding

constraints in structural design, and [15] to tailor simply-connected electrodes in piezo-transducers in order to reduce the electrical wiring requirements in such devices. It has been recently improved in [16] by incorporating a nonlinear heat source term, making the temperature in enclosed voids uniform over the whole structure, regardless of the void sizes, wall thickness, and locations.

40     Inspired also by the VTM, other authors have developed a similar approach based on the well-known electrostatic theory [17] that is able to cope with casting constraints [18] and stress constraints [19]. Others techniques developed for the last few years to eliminate enclosed voids are the following: a projection-based method [20], a feature-driven method [21], a particle diffusion-based method [22], and a bi-directional evolutionary structural optimization method [23]. This last work also uses some ideas coming from graphs, but in a different way as it is done here.

50     The aim of this work is to bring together the areas of topology optimization and graph theory to propose a new method that succeeds in avoiding the presence of internal or encapsulated holes in topology optimized structures. No advanced knowledge of graph theory is required by the reader to fully understand the idea we propose here, and to this end, we will introduce the preliminaries needed. Although our proposal was initially conceived to identify (and avoid) enclosed voids in structures, it may be extended to recognize isolated features of any materials in a design domain where coexisting two phases. In particular, it would be of great interest to detect “floating islands” and to control the number of them in the design of photonic devices [24], and to design efficiently connected two-phase electrode in piezoelectric transducers (this is actually a work in progress).

60     The layout of the paper is as follows. Section 2 is dedicated to providing a brief introduction to graph theory and examine the required concepts. Section 3 is devoted to presenting a method that successfully detects the number of enclosed holes in a design domain where coexisting two phases, a material phase and a void phase. In Section 4, a new formulation for structural design that includes the connectivity constraint over the void phase is proposed in the

framework of a topology optimization problem. The sensitivity analysis is also included here. Section 5 provides some numerical examples in 2d and 3d for minimum compliance with and without connectivity constraints. Finally, some conclusions and comments are provided in the last section.

## 70 **2. Some preliminaries on graphs**

Graph theory [25] is the branch of mathematics devoted to study graphs, which are formal mathematical structures used to model pairwise relations between its components. A graph is basically a set of vertices, also called nodes or points, some (or possibly all) of which connected by edges, also called links or lines. In the literature on this subject, it is customary to denote a graph as  $G = (V, E)$  where  $V$  is the set of vertices and  $E$  means the set of edges. Graphs are very present nowadays and the study of different paths in graphs has many applications in real-world problems. As vertices in a graph may abstractly represent objects, people, computers, whatever, graphs can be used to model many  
80 types of relations and processes in physical, biological and social systems.

Although we can find really complex structures of graphs, we consider here finite graphs without loops and multiple edges, and in particular, we focus on undirected graphs. In undirected graphs or just called simple graphs, edges link two vertices symmetrically because edges have no orientations. Figure 1a shows an example of a simple graph. An arbitrary number may be incorporated on each edge and therefore extend the concept of simple graphs to weighted graphs as in Figure 1b. In other words, a weighted graph is just an undirected graph with the property that for each edge, there is an associated positive number. This value, typically called weight,  $w_{ij}$ , tells us how strong the connection is  
90 between the nodes  $i - j$ , thus giving a measure of local connectivity.

In simple graphs, it is also assumed that all connections (whenever they exist) are equally important so they all have the same weight (equals 1) and the edges with weight zero are omitted, whereas in weighted graphs, weights may take arbitrary values.



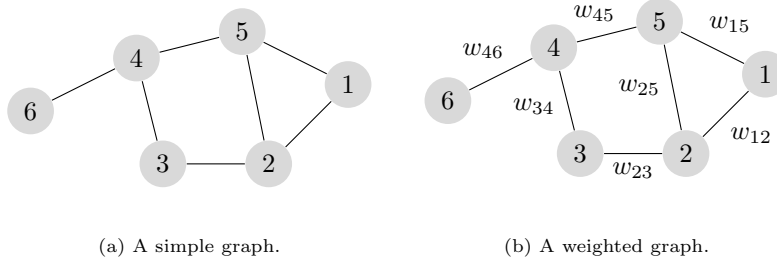


Figure 1: Examples of graphs.

Associated to a graph, we could define different matrices. And most importantly, making use of spectral theory for graphs [25], it is possible to study the properties of graphs in relationship to the eigenvalues or eigenvectors of such kind of matrices. Here we focus on the Laplacian matrix, and in particular, on the connection between the zero eigenvalue of that matrix and graph connectivity.

In a general way, given a weighted graph with  $n$  vertices, its (weighted) Laplacian matrix  $\mathcal{L}_{n \times n}$  is computed as follows:  $\mathcal{L}_{ij} = -w_{ij}$  if there is an edge linking the pair of (distinct) vertices  $i - j$  and  $\mathcal{L}_{ij} = 0$ , otherwise; and  $\mathcal{L}_{ii}$  is the sum of the weights on edges that leave from a vertex  $i$ . Here, we are assuming that  $w_{ij} \geq 0$ . In particular, (1) is that matrix for the example of Figure 1b. This helps highlight that the Laplacian matrix has important properties: it is symmetric, positive-semidefinite, and the sum of components of any row is zero, so the first eigenvalue is always null.

$$\mathcal{L} = \begin{pmatrix} w_{12} + w_{15} & -w_{12} & 0 & 0 & -w_{15} & 0 \\ -w_{21} & w_{21} + w_{23} + w_{25} & -w_{23} & 0 & -w_{25} & 0 \\ 0 & -w_{32} & w_{32} + w_{34} & -w_{34} & 0 & 0 \\ \vdots & \vdots & \vdots & \vdots & \vdots & \vdots \end{pmatrix} \quad (1)$$

The topology of the Laplacian matrix can be found in different contexts of structural mechanics, for instance, in discrete mechanical systems of masses and springs, as the one depicted in Figure 2. In such situations the equivalence is

direct, as the Laplacian matrix plays the role of the stiffness matrix there, just replacing the weights  $w_{ij}$  with the spring constants  $k_{ij}$ . We may find other analogies in difference finite schemes over the partial differential equation where the Laplace operator appears to explain a physical phenomenon like the small vibrations of a membrane, for instance.

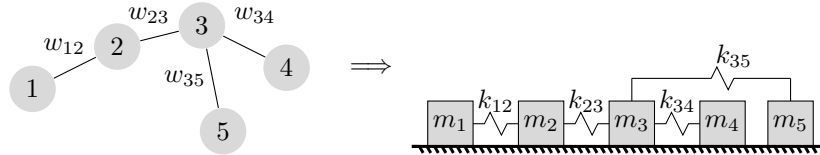


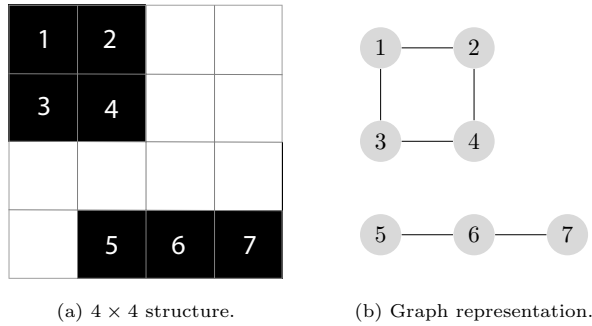
Figure 2: Equivalence between a weighted graph and a discrete mechanical system of masses and springs.

110 Another important concept to be considered is graph connectivity. We say that a graph is connected if there is a path linking any two of its vertices. The important point to note here is that exists a classical result of spectral graph theory that connects graph connectivity with an invariant of the Laplacian matrix. That result is due to M. Fiedler, and he showed, first for simple graphs [26] and later for weighted graphs with non-negative values on the edges [27], that the multiplicity of zero eigenvalue of the Laplacian matrix is equal to the number of connected components of a graph. Then, a graph is connected if and only if the second smallest Laplacian eigenvalue is positive. The term *algebraic connectivity* to refer such an eigenvalue was coined by Fiedler, and that is the  
 120 reason why it is also known in literature as Fiedler eigenvalue. This invariant plays a fundamental role in the field of spectral graph theory as it shows a measure of how well connected an overall graph is.

Some authors have showed interest in maximizing the weighted algebraic connectivity in different communications networks [28, 29, 30]. The reader is also referred to the survey [31] to know more about this spectral parameter, placing emphasis on bounds to the algebraic connectivity as a function of other

graph invariants. And special mention is required to its associated eigenvector (or Fiedler eigenvector), as it has many applications in the partitioning of meshes for parallel computing [32, 33].

130 In order to understand better our proposal, let us consider the coarse FE-mesh ( $4 \times 4$ ) in Figure 3a that we may interpret as a structure characterized by a binary density  $\rho \in \{0, 1\}$ , where white color means void ( $\rho = 0$ ) and black color denotes solid material ( $\rho = 1$ ).



$$\left( \begin{array}{cccc|ccc} 2 & -1 & -1 & 0 & & & \\ -1 & 2 & 0 & -1 & & & \\ -1 & 0 & 2 & -1 & & & \\ 0 & -1 & -1 & 2 & & & \\ \hline & & & & 1 & -1 & 0 \\ & & & & -1 & 1 & -1 \\ & & & & 0 & -1 & 1 \end{array} \right)$$

(c) Laplacian matrix of the solid phase.

Figure 3: Example of a graph associated to the solid phase in 0/1 structure.

Regarding the centroids of the solids elements as nodes of a particular graph (see Fig. 3b), its associated Laplacian matrix  $\mathcal{L} \in \mathbb{R}^{7 \times 7}$  (showed at Fig. 3c) is built in the same way as (1), where now the weights  $w_{ij}$  just take two possible values on: 1 when two black adjacent elements are connected and 0 in any other case. In this case, both the first and second eigenvalues are null, but not the third one, which means that the solid phase is formed by two connected  
 140 components. This highlights the fact that the connectivity of a structure may

be characterized by the multiplicity of the null eigenvalue of  $\mathcal{L}$ .

However, densities in topology optimization problems take continuous values in  $[0, 1]$ , so in order to create a graph associated to a general density, we need to introduce weights  $w_{ij}$  defined by

$$w_{ij} = \begin{cases} \rho_i \rho_j & \text{if } K_i \text{ and } K_j \text{ are adjacent elements,} \\ 0 & \text{otherwise,} \end{cases} \quad (2)$$

where  $K_i$  are the elements of the mesh, and  $\rho_i$  the densities on each element. With this definition, the associated graph has as many nodes as elements in the mesh, unlike the example of Figure 3, where only solid elements are considered as nodes.

This definition of weights implies that, for the structure of Figure 3a, the corresponding Laplacian matrix  $\mathcal{L} \in \mathbb{R}^{16 \times 16}$  would have 9 null lines, and the multiplicity of zero eigenvalue would not longer reflect the number of connected components of the structure. We will address this issue in the next section.

### 150 3. The algebraic connectivity method

As we mentioned at the introduction, the aim of this paper is to design topology optimized structures without inner holes. It is easy to realize that if an structure has an enclosed hole then the set corresponding to the void phase is not connected. Unfortunately, that also happens for structures without inner holes as in Figure 4a. However if we consider an extension of the design domain as in Figure 4b, then the void phase is connected now, so we can characterize the number of inner holes in structures through the number of connected components minus one of the void phase in the extended domain. So, structures without inner holes are identified as having connected graph associated with the  
 160 void phase of their extended structures. We will use the eigenvalue problem for the Laplacian matrix of the graph to impose this connectivity constraint.

As we are interested on the connectivity of the void phase, instead of considering a density  $\rho$ , we will use the density of the void phase, that is,  $1 - \rho$ . On the other hand, a penalization of gray areas with a parameter  $q$ , in the same spirit

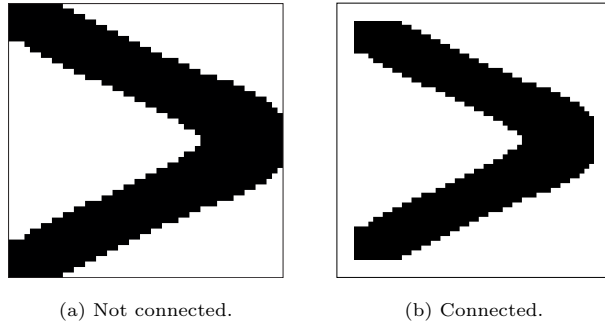


Figure 4: Connectivity of void phase.

as the SIMP does, is also incorporated; and finally, we introduce a small parameter  $W_{\min}$  to prevent that, eventually, an entire row of the Laplacian matrix is null (as we mentioned in the previous section). With all these considerations, we define the weights:

$$w_{ij} = \begin{cases} ((1 - \rho_i)(1 - \rho_j))^q (1 - W_{\min}) + W_{\min}, & \text{if } K_i \text{ and } K_j \text{ are adjacent,} \\ 0 & \text{otherwise.} \end{cases} \quad (3)$$

Although we have tried with different sets of values for the above tuning parameters, in our experience, the best choice for both of them is  $q = 6$  and  $W_{\min} = 10^{-5}$ . Note that these weights are referred to the structure in the extended domain, where the density is considered as zero in the extension.

The role of  $W_{\min}$  is to avoid null lines in the Laplacian matrix, and has an undesirable effect on their eigenvalues: now, only the first eigenvalue is null. However, as we show below (see Table 1), the number of eigenvalues *close* to zero are still equal to the number of connected components of the void phase.

Therefore, for regular rectangular meshes, the matrix  $\mathcal{L}(\boldsymbol{\rho})$  may be obtained by assembling all elemental contributions between two adjacent nodes  $i - j$ , which are expressed as

$$\mathcal{L}_{i-j} = w_{ij} \begin{pmatrix} 1 & -1 \\ -1 & 1 \end{pmatrix}.$$

170 And finally, we build the matrix  $\mathbf{M}(\boldsymbol{\rho}) \in \mathbb{R}^{n \times n}$  as the global (lumped) mass

matrix that stores in its diagonal the values  $(1 - \rho_i)|K_i|$ , being  $|K_i|$  the measure of the element  $K_i$  of the mesh, and  $n$  the number of nodes in the graph, that coincides with the number of the finite elements in the mesh.

For a general mesh, these matrices can be build using the pseudocode showed in Algorithm 1.

**Algorithm 1:** Pseudocode to build matrices  $\mathcal{L}$  and  $\mathbf{M}$ .

**Data:** Density  $\rho \in [0, 1]$ ; Mesh  $\tau_h = \{K_i\}_i$  //  $\rho$  is a vector

**Result:** Matrices  $\mathcal{L}(\rho) = (l_{ij})$  and  $\mathbf{M}(\rho) = (m_{ij})$

Initialization:  $l_{ij} = 0$ ;  $m_{ij} = 0$ ;

**for**  $i \leftarrow 1$  **to**  $n$  **do**

$m_{ii} \leftarrow (1 - \rho_i)|K_i|$

**for**  $j \in \mathcal{N}_i = \{k : K_k \text{ is adjacent to } K_i\}$  **do**

$l_{ij} \leftarrow -(((1 - \rho_i)(1 - \rho_j))^q (1 - W_{\min}) + W_{\min})$

$l_{ii} \leftarrow l_{ii} - l_{ij}$

**end**

**end**

To avoid some problems due to the null eigenvalue, it is convenient to apply a shifting in the eigenvalue problem, which leads to consider the following eigenvalue problem: find  $(\lambda_j, \Phi_j)$  such that

$$\begin{aligned} (\mathcal{L}(\rho) - (\lambda_j - 1)\mathbf{M}(\rho))\Phi_j &= \mathbf{0}, \\ \Phi_j^T \mathbf{M}(\rho) \Phi_j &= 1, \end{aligned} \tag{4}$$

paying now attention to the multiplicity of the unit eigenvalue. Here,  $(\lambda_j, \Phi_j)$  is the pair eigenvalue and its associated  $\mathbf{M}$ -orthonormal eigenvector, respectively.

To illustrate how our method succeeds in determining the number of isolated void areas in a certain domain, let us consider the images in Table 1. They correspond with three optimized structures for certain boundary conditions in loads and displacements:  $\rho_A$ , with some remaining gray areas,  $\rho_B$  purely black and white, and  $\rho_C$  with more gray areas. When solving the eigenproblem (4) for  $\rho_B$ , it is observed the following: the first eigenvalue is one; the second and the third eigenvalues are almost one (they are not because of the parameter  $W_{\min}$ ),

and the fourth one is much greater than one. So we can conclude that there are three void areas since the algebraic multiplicity of  $\lambda \approx 1$  is three as well. Same conclusions can be drawn on solving the eigenproblem for  $\rho_A$  when using two different values of the power  $q$ . Moreover, it is observed that the higher the power  $q$ , the lower the fourth eigenvalue, but it does not really mind for our interests so far. Also, if the structure has more gray areas like  $\rho_G$ , higher values of  $q$  are needed to identify the void areas. Otherwise, we will get the risk of seeing all the domain as a whole, without distinguishing the solid from the void. This happens when  $q = 1$ , as both the second and third eigenvalues are far from the unit value.

	$\rho_A, q = 1$	$\rho_A, q = 6$	$\rho_B$	$\rho_G, q = 1$	$\rho_G, q = 6$
$\lambda_1$	1	1	1	1	1
$\lambda_2$	1.0004	1.0004	1.0003	1.8923	1.0004
$\lambda_3$	1.0007	1.0007	1.0005	2.6232	1.0007
$\lambda_4$	19.888	1.2500	20.565	19.778	1.0158

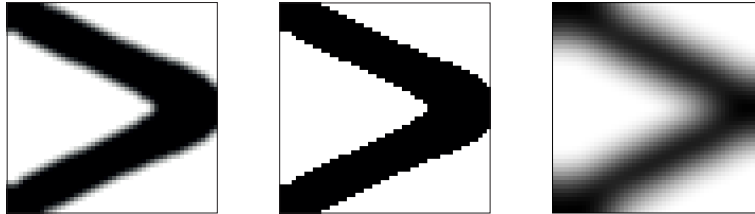


Table 1: The first four eigenvalues for the problem (4) when considering the optimized structures  $\rho_A$  (with some gray areas),  $\rho_B$  (black and white) and  $\rho_G$  (with many gray areas).

In Table 2, we show the effect of considering the extended domain (an small outside frame of void phase of three elements size). In this case, we get the first eigenvalue equal to one, and the second very close to one, which identifies two disconnected void areas (a inner hole, indeed). And, as before, the first eigenvalue far from one is smaller as  $q$  is higher.

In the next section, we will see how this method, that will be referred as the algebraic connectivity method (ACM), can be used to avoid the formation of

	$\rho_C, q = 1$	$\rho_C, q = 6$	$\rho_D$
$\lambda_1$	1	1	1
$\lambda_2$	1.0037	1.0027	1.0022
$\lambda_3$	1.9690	1.2613	1.9597

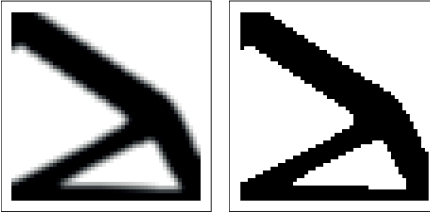


Table 2: The first three eigenvalues for the problem (4) when considering the optimized structures  $\rho_C$  (with some gray areas) and  $\rho_D$  (black and white).

enclosed holes in topology optimized structures.

#### 4. Problem formulation and sensitivity analysis

Having in mind the considerations of the previous section, the problem formulation for minimum compliance that incorporates void-phase connectivity may be written as

$$\begin{aligned}
 & \min_{\rho \in [0,1]} c = \mathbf{F}^T \mathbf{U} \\
 \text{subject to: } & \left\{ \begin{array}{ll} \tilde{\rho} & = \mathbf{H}(\rho) \quad (\text{density filter}) \\ \hat{\rho} & = \mathbf{P}(\tilde{\rho}) \quad (0/1 \text{ projection}) \\ \mathbf{K}(\hat{\rho})\mathbf{U} & = \mathbf{F} \quad (\text{state equation}) \\ \mathbf{v}^T \hat{\rho} & \leq V_0 |\Omega| \quad (\text{volume constraint}) \end{array} \right. \\
 & \left\{ \begin{array}{ll} \left( \mathcal{L}(\hat{\rho}^\sharp) - (\lambda_2 - 1)\mathbf{M}(\hat{\rho}^\sharp) \right) \Phi_2 & = \mathbf{0} \quad (\text{auxiliary eigenproblem}) \\ \Phi_2^T \mathbf{M}(\hat{\rho}^\sharp) \Phi_2 & = 1 \quad (\mathbf{M}\text{-orthonormalization}) \\ \lambda_2 & > 1 \quad (\text{connectivity constraint}) \end{array} \right.
 \end{aligned}$$

where  $\mathbf{K}$  is the global stiffness matrix,  $\mathbf{U}$  and  $\mathbf{F}$  are the global displacements and force vectors, respectively;  $\mathbf{v}$  is a vector containing the measure of the elements,  $V_0$  is the volume fraction, and  $|\Omega|$  is the measure of the design domain;  $\tilde{\rho}$  is the filtered density;  $\hat{\rho}$  is the projected (filtered) density; and  $\hat{\rho}^\sharp$  corresponds to the extension of  $\hat{\rho}$  to the extended domain with null values.

Here, SIMP method [34] is used to penalize intermediate densities and the



filtered density at element  $K_e$  is defined by

$$\tilde{\rho}_e = \frac{\sum_i d_e(\mathbf{x}_i)\rho_i}{\sum_i d_e(\mathbf{x}_i)},$$

where  $\mathbf{x}_i$  is the barycenter of element  $K_i$ , and the weighting function  $d_e(\mathbf{x}_i)$  is given by the cone-shape function

$$d_e(\mathbf{x}_i) = \max\{R - \|\mathbf{x}_i - \mathbf{x}_e\|, 0\}.$$

where  $R$  is the filter radius. By using this density filter, proposed in [35, 36], the  
 210 above finite-dimensional mathematical problem is well-posed, obtaining mesh-  
 independent solutions, a fact that was mathematically proved by Bourdin [35].

However, in the absence of projection techniques that force 0/1 designs ([37, 38, 39]), final layouts often exhibit some gray areas in the transition from material phase to void phase over the distance determined by the chosen filter radius. A thresholding projection method is then used to reduce intermediate density values, forcing, in this way, to obtain closer 0/1 solutions. Here it is performed using a continuation method with the smoothed Heaviside function proposed in [39]

$$\hat{\rho}_e \equiv P(\tilde{\rho}_e; \beta, \eta) = \frac{\tanh(\beta\eta) + \tanh(\beta(\tilde{\rho}_e - \eta))}{\tanh(\beta\eta) + \tanh(\beta(1 - \eta))},$$

where  $\hat{\rho}_e$  is the projected density of element  $K_e$ , the parameter  $\beta$  determines the sharpness of the projection and  $\eta \in [0, 1]$  is the threshold parameter. All densities whose value is lower than  $\eta$  are approximate to 0, and the ones whose value is bigger than this parameter are approximate to 1. The specific values of these parameters will be mentioned at Section 5.

Regarding the condition  $\lambda_2 > 1$ , it is treated here as  $\lambda_2 \geq \lambda_2^{\min}$ , where the value of the parameter  $\lambda_2^{\min}$  would be enough if it was around 1.15, in our experience, to avoid the formation of inner holes.

220 Focusing on the sensitivity analysis now, it does not truly entail any extra difficulties and just the derivation concerning the connectivity constraint is carefully mentioned. It is corresponds to computing the sensitivity of either a single

or repeated eigenvalue that is well-known. At this point, it is convenient to remember that we cannot compute sensitivities for multiple eigenvalues as they are not differentiable, but there exist formulae for computing the directional derivatives (and, in particular, the partial derivatives, which is what is required by the numerical algorithm). These expressions can be found in [40].

An important observation is the fact that  $\lambda_2$  never switches to the first (always of value one) eigenvalue due to the parameter  $W_{\min}$ , which always forces  $\lambda_2$  to stay over 1. Of course, both values may be really close during some iterations, but in such cases we have corroborated that the derivative formulas considering they are repeated eigenvalues are virtually the same as they are not. It seems to indicate that from a practical point of view they can be treated as single eigenvalues, and that  $\lambda_2$  may switch to the third eigenvalue only.

In case it was simple, and by differentiating Eq. (4) we arrive at

$$\frac{\partial \lambda_2}{\partial \hat{\rho}_e} = \Phi_2^T \left( \frac{\partial \mathcal{L}}{\partial \hat{\rho}_e} - (\lambda_2 - 1) \frac{\partial \mathbf{M}}{\partial \hat{\rho}_e} \right) \Phi_2.$$

If the second eigenvalue appears repeated ( $\lambda_2 \approx \lambda_3$ )<sup>1</sup>, then the formulas for eigenvalues derivatives may be expressed as [41, 42, 43]

$$\frac{\partial \lambda_2}{\partial \hat{\rho}_e} = \min(\text{diag}(\Lambda_{\mathbf{p}})), \quad \frac{\partial \lambda_3}{\partial \hat{\rho}_e} = \max(\text{diag}(\Lambda_{\mathbf{p}})).$$

$\Lambda_{\mathbf{p}}$  is the solution of the small ( $2 \times 2$ ) eigenproblem

$$\mathbf{D}\Gamma = \Gamma\Lambda_{\mathbf{p}}, \quad \mathbf{D} = \Xi^T \left( \frac{\partial \mathcal{L}}{\partial \hat{\rho}_e} - (\lambda_2 - 1) \frac{\partial \mathbf{M}}{\partial \hat{\rho}_e} \right) \Xi, \quad \Gamma^T \Gamma = \mathbf{I}_2,$$

where  $\Xi = [\Phi_2 \ \Phi_3]$ ,  $\Gamma$  is an orthogonal matrix and  $\mathbf{I}_2$  is the identity matrix.

Finally, in any of both cases

$$\frac{\partial \lambda_2}{\partial \rho_e} = \frac{\partial \lambda_2}{\partial \hat{\rho}_e} \frac{\partial \hat{\rho}_e}{\partial \tilde{\rho}_e} \frac{\partial \tilde{\rho}_e}{\partial \rho_e},$$

where  $\frac{\partial \hat{\rho}_e}{\partial \tilde{\rho}_e} \frac{\partial \tilde{\rho}_e}{\partial \rho_e}$  represents the standard modification of partial derivatives due to filtering and projection. Note that  $\rho_e^\# = \hat{\rho}_e$  for elements of the original mesh,

---

<sup>1</sup>Numerically we have used  $|\lambda_2 - \lambda_3| < 10^{-5}$ .

and  $\rho_e^\sharp = 0$  on the elements of the extension, so the partial derivatives do not change.

Once all the partial derivatives have been computed, the discretized problem  
240 is numerically solved by MMA [44], a non-linear programming solver that is widely  
used in structural optimization problems.

## 5. Numerical examples

This section is devoted to show some numerical examples that corroborate  
our method. Some of the optimization parameters used are the same for all of  
them. In particular, we have used unit side elements and an extension frame of  
three elements size. With regard to the connectivity constraint, a continuation  
strategy has been implemented, beginning with  $\lambda_2 > 1.05$  and ending with  
 $\lambda_2 > 1.15$ , increasing the value of the eigenvalue in 0.01 for each 50 iterations.  
Concerning projection parameters,  $\eta = 0.5$  and  $\beta$  is gradually increased from  
250 2 to 8 at every 50 iterations, beginning when the iterative process starts to  
stabilize, which means approximately after 300 iterations.

### 5.1. 2d examples

We start considering two examples in 2d, first, a cantilevered beam with a  
load applied in the middle point and second, the same structure when the load  
is applied in the lower right corner. Both examples, and specially the former,  
have been widely studied using some of the connectivity strategies described in  
Section 1. For these two examples, we have used different aspect ratios between  
horizontal and vertical dimensions. The volume fraction is  $V_0 = 0.4$  and the  
filter radius is  $R = 3.6$  which corresponds to a filter size of 3.6 elements in any  
260 direction. Focusing on the simulations, for the example in Figure 5a, the opti-  
mized compliance structure is already connected in the void phase. Therefore,  
the fact of imposing the connectivity constraint does not change anything, since  
the same layout is obtained in Figure 5b, as expected. However, when changing  
the aspect ratio, optimized compliance designs exhibit holes inside the domain

to maximize the stiffness. Now, forcing that void phase to be connected, new designs are obtained that obviously are a bit worse, 7% and 21% in Figures 5c and 5e, respectively, in terms of compliance, but they satisfy the connectivity requirements. Similar conclusions can be derived from the second example in Figure 6. In this case, the objective function increases its value in the percentages 3.5%, 8% and 13%, respectively, as the horizontal dimension does as well. Although this approach satisfactorily works for different starting points, in our experience the one which uses less iterations corresponds to taking a solid rectangle (of prescribed volume fraction) that connects the clamped boundary condition with the load in any of the two cases. Indeed, it is observed that the connectivity constraint is active at the end of the optimization process, finishing with  $\lambda_2 = 1.15$  in both examples. Figure 7 shows the convergence history of the compliance and the connectivity constraint for Figure 6f.

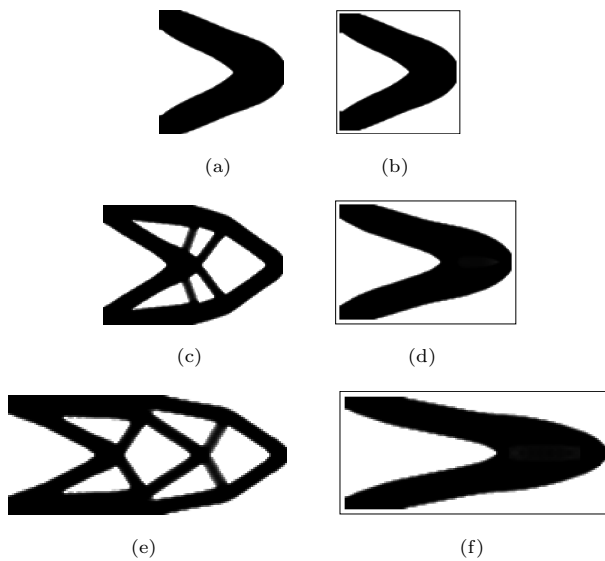


Figure 5: Example of a cantilevered beam with a load in the middle point. (a), (c) and (e) are minimum compliance designs; (b), (d) and (f) are the same but forcing that void phase to be connected in an extended domain.

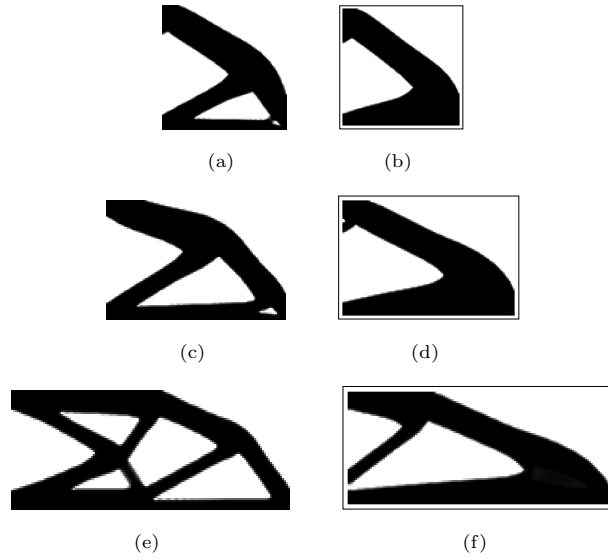


Figure 6: Example of a cantilevered beam with a load in the lower right. (a), (c) and (e) are minimum compliance designs; (b), (d) and (f) are the same but forcing that void phase to be connected in an extended domain.

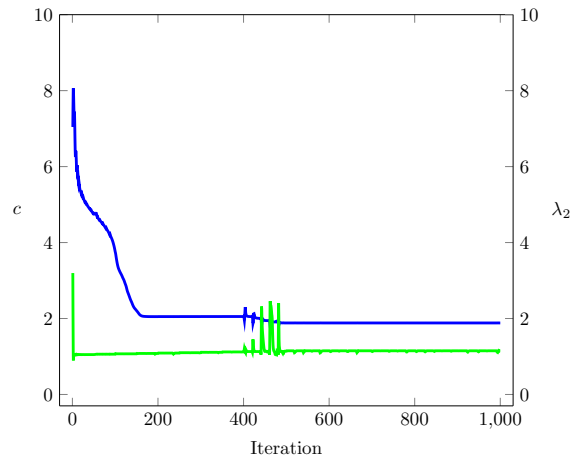


Figure 7: Convergence history of both compliance and connectivity constraint for the case study of Fig. 6f.

### 5.2. 3d examples

The following two 3d examples appeared for the first time in the context  
280 of connectivity constraints in [9, 10], and they have also been simulated later  
in some of the references cited in section 1. To run these examples, we have  
adapted the existing 3d code [45].

The first one corresponds to a hexahedron simply supported at the four  
corners at the bottom face. A unit vertical point load is applied at the center  
of the bottom face (see Fig. 8). The design domain is discretized by  $40 \times 40 \times 20$   
eight-node cubic elements. Two layers at the bottom surface are chosen as  
passive volume that keeps solid during the optimization process. The volume  
fraction is  $V_0 = 0.3$  and the filter radius is  $R = 2$ .

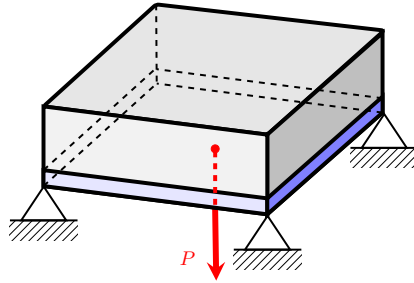


Figure 8: Design domain and boundary conditions for the third example.

As we can observe in Figure 9, both optimized structures, minimum com-  
290 pliance structure with and without connectivity constraints, are quite similar  
in appearance, but in the absence of connectivity constraints a small hole get  
trapped inside the domain (Fig. 9a). Forcing again the void phase to be con-  
nected, the objective function is just incremented in 5.6%, what it means a  
really good trade-off between stiffness and connectivity, with a final value of  
 $\lambda_2 = 1.36$ .

The final case study corresponds to a cantilevered beam subjected to a torque  
load applied on the right end face. The design domain is discretized by  $20 \times$   
 $60 \times 20$  cubic elements. Two layers of elements at both ends of the structure

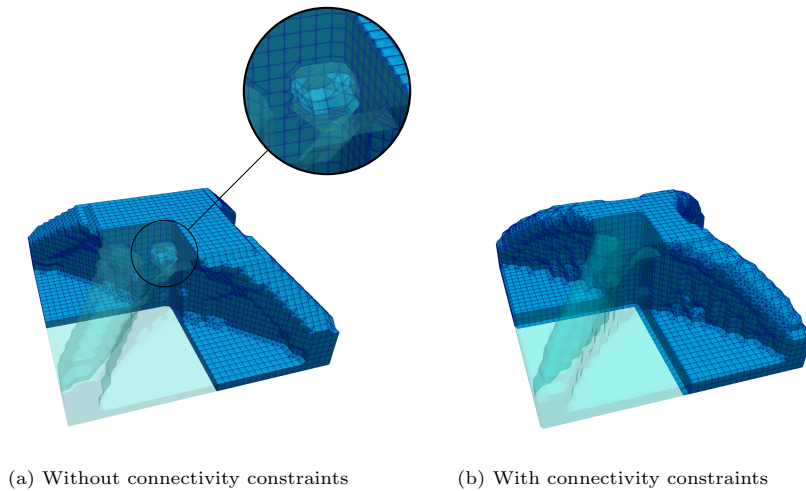


Figure 9: Minimum compliance structures for the example of Fig. 8.

are chosen as passive volume, that remains solid as before. The volume fraction  
 300 is  $V_0 = 0.3$  and the filter radius is  $R = 2$ .

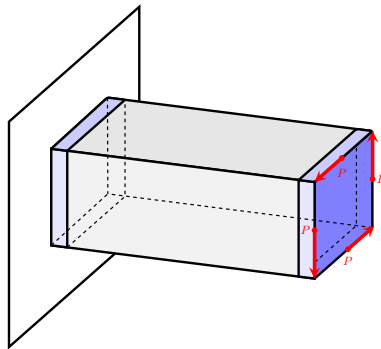


Figure 10: Design domain and boundary conditions for the fourth example.

It is well known that for an enough volume fraction of material, minimum compliance design corresponds to a thin-walled cantilever, containing in this way a very big hole inside the whole domain, as it is depicted in Figure 11a. Imposing now a void connectivity constraint, a new truss-like structure is shown in Figure 11b, letting the hole connect to the void frame, but at the expenses of

loosing stiffness. In this case, the compliance is increased in 45% and  $\lambda_2 = 1.73$ .

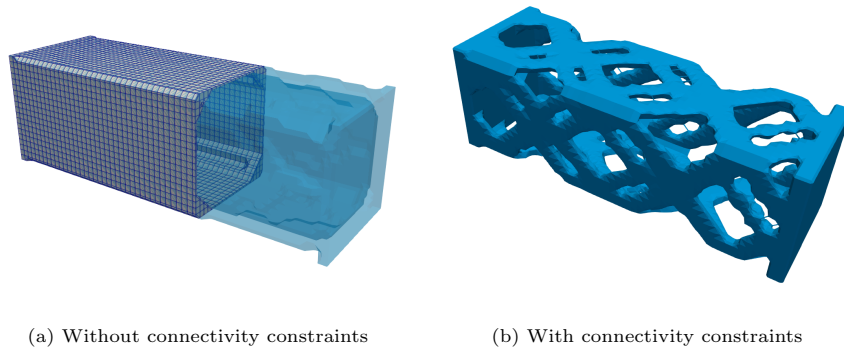


Figure 11: Minimum compliance structures for the example of Fig. 10.

## 6. Conclusions and future lines

In this work, the problem of avoiding the formation of inner holes in topology optimized structures has been treated from a more mathematical perspective than it has been done to date. The strategy consisted in considering the centroids of the finite elements in a mesh as nodes, those conforming a graph according to the connections of such elements in the mesh. Based on known results of spectral graph theory concerning graph connectivity, it is first developed a method that succeeds in determining the number of non-connected void areas in a design domain where coexisting two phases. Often, they both are material and void phases, but it works as the independence of the physical meaning of the phases. Extending that idea, it is also proposed a TO-based formulation to prevent the formation of inner holes in minimum compliance structures. This has been illustrated through several convincing examples in 2d and in 3d. These two above contributions lie in a better insight into the so-called algebraic connectivity, the first non-zero eigenvalue of the Laplacian matrix, which measures the overall graph connectivity. We consider they are still some pending issues to fully understand this eigenvalue that are, however, far from the scope of this



work. For this reason we will continue to deepen in this invariant in a near future. Also we plan to apply these ideas to other physical contexts of interest.

**Acknowledgements** Authors acknowledge financial support from the Spanish Ministerio de Ciencia e Innovación through grant PID2020-116207GB-I00, Junta de Castilla - La Mancha through grant SBPLY/19/180501/000110, and European Regional Development Fund 2018/11744.

### 330 **References**

- [1] M. P. Bendsøe, O. Sigmund, *Topology optimization: theory, methods, and applications*, 2nd Edition, Springer, 2003.
- [2] J. Liu, A. Gaynor, S. Chen, et al., Current and future trends in topology optimization for additive manufacturing, *Struct Multidisc Optim* 57 (2018) 2457–2483.
- [3] L. Meng, W. Zhang, D. Quan, et al., From topology optimization design to additive manufacturing: Today’s success and tomorrow’s roadmap, *Arch Computat Methods Eng* 27 (2020) 805–830.
- [4] A. Gersborg, C. Andreasen, An explicit parameterization for casting constraints in gradient driven topology optimization, *Struct Multidisc Optim* 44 (2011) 875–881.
- [5] J. K. Guest, M. Zhu, Casting and milling restrictions in topology optimization via projection-based algorithms, *ASME Design Engineering Technical Conference* 3 (2012) 913–920.
- [6] Y. Sato, T. Yamada, K. Izui, S. Nishiwaki, Manufacturability evaluation for molded parts using fictitious physical models, and its application in topology optimization, *Int J Adv Manuf Technol* 92 (2017) 1391–1409.
- [7] G. H. Yoon, Structural topology optimization of layout and raster angle for additive manufacturing technology with the shadow density filter, *Computers & Structures* 256 (2021) 106637.

- [8] H. Y. Lee, M. Zhu, J. K. Guest, Topology optimization considering multi-axis machining constraints using projection methods, *Computer Methods in Applied Mechanics and Engineering* 390 (2022) 114464.
- [9] S. Liu, Q. Li, W. Chen, L. Tong, G. Cheng, An identification method for enclosed voids restriction in manufacturability design for additive manufacturing structures, *Front Mech Eng* 10 (2) (2015) 126–137.
- [10] Q. Li, W. Chen, S. Liu, L. Tong, Structural topology optimization considering connectivity constraint, *Struct Multidisc Optim* 54 (2016) 971–984.
- [11] M. Osanov, J. Carstensen, E. Tromme, J. Guest, C. Williams, Topology optimization for additive manufacturing: New projection-based design algorithms, in: *Proceedings of 17th AIAA/ISSMO Multidisciplinary Analysis and Optimization Conference, Aviation 2016*, AIAA, Washington D.C., 2016, pp. 1–9.
- [12] N. Jenkins, K. Maute, An immersed boundary approach for shape and topology optimization of stationary fluid-structure interaction problems, *Struct Multidisc Optim* 54 (2016) 1191–1208.
- [13] R. Behrou, R. Ranjan, J. K. Guest, Adaptive topology optimization for incompressible laminar flow problems with mass flow constraints, *Computer Methods in Applied Mechanics and Engineering* 346 (2019) 612–641.
- 370 [14] Q. Li, W. Chen, S. Liu, H. Fan, Topology optimization design of cast parts based on virtual temperature method, *Computer-Aided Design* 94 (2018) 28–40.
- [15] A. Donoso, J. K. Guest, Topology optimization of piezo modal transducers considering electrode connectivity constraints, *Computer Methods in Applied Mechanics and Engineering* 356 (2019) 101–115.
- [16] Y. Luo, O. Sigmund, Q. Li, S. Liu, Additive manufacturing oriented topology optimization of structures with self-supported enclosed voids, *Computer Methods in Applied Mechanics and Engineering* 372 (2020) 113385.

- 380 [17] C. Wang, B. Xu, Q. Meng, J. Rong, Y. Zhao, Numerical performance of poisson method for restricting enclosed voids in topology optimization, *Computers & Structures* 239 (2020) 106337.
- [18] C. Wang, B. Xu, Q. Meng, J. Rong, Y. Zhao, Topology optimization of cast parts considering parting surface position, *Advances in Engineering Software* 149 (2020) 102886.
- [19] C. Wang, B. Xu, Z. Duan, et al, Structural topology optimization considering both performance and manufacturability: strength, stiffness, and connectivity, *Struct Multidisc Optim* 63 (2021) 1427–1453.
- 390 [20] A. T. Gaynor, T. E. Johnson, Eliminating occluded voids in additive manufacturing design via a projection-based topology optimization scheme, *Additive Manufacturing* 33 (2020) 101149.
- [21] L. Zhou, W. Zhang, Topology optimization method with elimination of enclosed voids, *Struct Multidisc Optim* 60 (2019) 117–136.
- [22] G. Sabiston, I. Kim, Void region restriction for additive manufacturing via a diffusion physics approach, *Int J Numer Methods Eng* 121 (2020) 4347–4373.
- [23] Y. Xiong, S. Yao, Z.-L. Zhao, Y. M. Xie, A new approach to eliminating enclosed voids in topology optimization for additive manufacturing, *Additive Manufacturing* 32 (2020) 101006.
- 400 [24] R. E. Christiansen, O. Sigmund, Inverse design in photonics by topology optimization: tutorial, *J. Opt. Soc. Am. B* 38 (2) (2021) 496–509.
- [25] F. R. K. Chung, *Spectral Graph Theory*, American Mathematical Society, 1997.
- [26] M. Fiedler, Algebraic connectivity of graphs, *Czechoslovak Mathematical Journal* 23 (2) (1973) 298–305.

- [27] M. Fiedler, Laplacian of graphs and algebraic connectivity, *Combinatorics and Graph Theory* 25 (1989) 57–70.
- [28] H. Zhang, J. Wei, P. Yi, X. Hu, Projected primal–dual gradient flow of augmented lagrangian with application to distributed maximization of the algebraic connectivity of a network, *Automatica* 98 (2018) 34–41.
- 410 [29] Y. Zheng, S. Zhao, Y. Liu, Y. Li, Q. Tan, N. Xin, Weighted algebraic connectivity maximization for optical satellite networks, *IEEE Access* 5 (2017) 6885–6893.
- [30] H. Nagarajan, S. Rathinam, S. Darbha, K. R. Rajagopal, Synthesizing robust communication networks for uavs, in: *2012 American Control Conference (ACC)*, 2012, pp. 3730–3735.
- [31] N. M. M. de Abreu, Old and new results on algebraic connectivity of graphs, *Linear Algebra and its Applications* 423 (1) (2007) 53–73.
- [32] H. Simon, Partitioning of unstructured problems for parallel processing, *Computing Systems in Engineering* 2 (2) (1991) 135–148.
- 420 [33] D. A. Spielman, S.-H. Teng, Spectral partitioning works: Planar graphs and finite element meshes, *Linear Algebra and its Applications* 421 (2) (2007) 284–305.
- [34] M. P. Bendsøe, O. Sigmund, Material interpolation schemes in topology optimization, *Arch Appl Mech* 69 (1999) 635–654.
- [35] B. Bourdin, Filters in topology optimization, *Int J Number Meth Engng* 50 (9) (2001) 2143–2158.
- [36] T. E. Bruns, D. A. Tortorelli, Topology optimization of nonlinear elastic structures and compliant mechanisms, *Comput Methods Appl Mech Engrg* 190 (26–27) (2001) 3443–3459.

- 430 [37] J. K. Guest, J. H. Prévost, T. Belytschko, Achieving minimum length scale in topology optimization using nodal design variables and projection functions, *International Journal for Numerical Methods in Engineering* 61 (2) (2004) 238–254.
- [38] O. Sigmund, Morphology-based black and white filters for topology optimization, *Structural and Multidisciplinary Optimization* 33 (4) (2007) 401–424.
- [39] F. Wang, B. S. Lazarov, O. Sigmund, On projection methods, convergence and robust formulations in topology optimization, *Struct Multidisc Optim* 43 (6) (2011) 767–784.
- 440 [40] E. J. Haug, K. K. Choi, V. Komkov, Design sensitivity analysis of structural systems, *Mathematics in Science and Engineering*, Volume 177, Academic press, 1986.
- [41] A. Seyranian, E. Lund, N. Olhoff, Multiple eigenvalues in structural optimization problems, *Structural Optimization* 8 (1994) 207–227.
- [42] J. S. Jensen, N. L. Pedersen, On maximal eigenfrequency separation in two-material structures: the 1d and 2d scalar cases, *Journal of Sound and Vibration* 289 (4) (2006) 967–986.
- [43] G. Yoon, A. Donoso, J. Bellido, D. Ruiz, Highly efficient general method for sensitivity analysis of eigenvectors with repeated eigenvalues without  
450 passing through adjacent eigenvectors, *International Journal for Numerical Methods in Engineering* 121 (20) (2020) 4473–4492.
- [44] K. Svanberg, The method of moving asymptotes—a new method for structural optimization, *Int J Number Meth Engng* 24 (2) (1987) 359–373.
- [45] K. Liu, A. Tovar, An efficient 3d topology optimization code written in matlab, *Struct. Multidiscip. Optim.* 50 (6) (2014) 1175–1196.